



ARL-TR-9378 • Jan 2022



Development of Subscale Tester for High-Cycle Fatigue Evaluation

by Travis Wagner and Denise Yin

Approved for public release: distribution unlimited.

NOTICES

Disclaimers

The findings in this report are not to be construed as an official Department of the Army position unless so designated by other authorized documents.

Citation of manufacturer's or trade names does not constitute an official endorsement or approval of the use thereof.

Destroy this report when it is no longer needed. Do not return it to the originator.



Development of Subscale Tester for High-Cycle Fatigue Evaluation

Travis Wagner

Army Educational Outreach Program

College Qualified Leaders, Rochester Institute of Technology

Denise Yin

Weapons and Materials Directorate, DEVCOM Army Research Laboratory

REPORT DOCUMENTATION PAGE

*Form Approved
OMB No. 0704-0188*

Public reporting burden for this collection of information is estimated to average 1 hour per response, including the time for reviewing instructions, searching existing data sources, gathering and maintaining the data needed, and completing and reviewing the collection information. Send comments regarding this burden estimate or any other aspect of this collection of information, including suggestions for reducing the burden, to Department of Defense, Washington Headquarters Services, Directorate for Information Operations and Reports (0704-0188), 1215 Jefferson Davis Highway, Suite 1204, Arlington, VA 22202-4302. Respondents should be aware that notwithstanding any other provision of law, no person shall be subject to any penalty for failing to comply with a collection of information if it does not display a currently valid OMB control number.

PLEASE DO NOT RETURN YOUR FORM TO THE ABOVE ADDRESS.

1. REPORT DATE (DD-MM-YYYY) January 2022		2. REPORT TYPE Technical Report		3. DATES COVERED (From - To) 5/21/2019 – 5/28/2021	
4. TITLE AND SUBTITLE Development of Subscale Tester for High-Cycle Fatigue Evaluation				5a. CONTRACT NUMBER	
				5b. GRANT NUMBER	
				5c. PROGRAM ELEMENT NUMBER	
6. AUTHOR(S) Travis Wagner and Denise Yin				5d. PROJECT NUMBER	
				5e. TASK NUMBER	
				5f. WORK UNIT NUMBER	
7. PERFORMING ORGANIZATION NAME(S) AND ADDRESS(ES) DEVCOM Army Research Laboratory ATTN: FCDD-RLW-MF Aberdeen Proving Ground, MD 21005				8. PERFORMING ORGANIZATION REPORT NUMBER ARL-TR-9378	
9. SPONSORING/MONITORING AGENCY NAME(S) AND ADDRESS(ES)				10. SPONSOR/MONITOR'S ACRONYM(S)	
				11. SPONSOR/MONITOR'S REPORT NUMBER(S)	
12. DISTRIBUTION/AVAILABILITY STATEMENT Approved for public release: distribution unlimited.					
13. SUPPLEMENTARY NOTES ORCID ID: Denise Yen, 0000-0003-4184-5336					
14. ABSTRACT This report documents the development and technical validation of a subscale high-cycle fatigue tester as a materials characterization tool useful for generating Wöhler (stress-life; S-N) diagrams. The instrument operates under constant amplitude (displacement) loading and subjects flat-sheet specimens with modified Krouse-type geometry to fixed cantilever bending mode with a stress ratio between -1 (“fully reversed”) and 0 (“pulsating tension”). A LabVIEW program provides a user interface that displays a direct read-out of the number of cycles and saves a record of the data to a comma-separated-value file for further processing. Here we report the setup and operation of the instrument as well as details regarding specimen design and preparation. In particular, we investigate aluminum alloy 6061-T6 under fully reversed bending conditions and a 25-Hz frequency. Tests are carried out with guidance from ASTM standards B593 and E739. Corroborated by comparisons with literature data, the system can be used for effective implementation for at least aluminum alloys, although other classes of materials should be validated for as well (e.g., steels, to improve instrument robustness and versatility). Subscale fatigue testing is beneficial for limited material volumes, particularly under circumstances of high specimen preparation costs in the conventional, full-scale counterpart.					
15. SUBJECT TERMS high-cycle fatigue, bending fatigue, aluminum alloy, small-scale mechanical testing, fracture					
16. SECURITY CLASSIFICATION OF:			17. LIMITATION OF ABSTRACT UU	18. NUMBER OF PAGES 28	19a. NAME OF RESPONSIBLE PERSON Denise Yin
a. REPORT Unclassified	b. ABSTRACT Unclassified	c. THIS PAGE Unclassified			19b. TELEPHONE NUMBER (Include area code) (410) 306-0988

Contents

List of Figures	iv
Acknowledgments	v
1. Introduction	1
2. Description of Instrument	1
2.1 Basic Operation	1
2.2 Mechanical Linkage	2
2.3 Description of Specimen	5
2.3.1 Design	5
2.3.2 Stress Distribution	6
2.3.3 Specimen Preparation	9
2.4 Test Setup Procedure	10
2.4.1 Stress Amplitude Adjustment	10
2.4.2 Center of Loading Adjustment	11
2.5 Fracture Mechanics	11
2.6 Maintenance/Wear	12
2.7 Electronics	13
2.7.1 Overview	13
2.7.2 LabVIEW Code	13
2.8 Instrument Validation	15
3. Size Effect	17
4. Conclusion	17
5. References	18
List of Symbols, Abbreviations, and Acronyms	20
Distribution List	21

List of Figures

Fig. 1	Overview images of the fatigue tester with key parts labeled in a) rendered form (top-down) and b) photographic form (angled)	3
Fig. 2	Rendered CAD image showing counter-rotation adjustment of the cam housing.....	3
Fig. 3	Schematic showing specimen geometry (millimeters). The two holes are machined with imperial units: 1/32 and 1/8 inch (left to right); equivalent dimensions shown in metric.....	5
Fig. 4	Rendered CAD images showing the clamping mechanism with a) a specimen present (orange) and b) the specimen missing with an angled view of the mobile grip. The stationary grip is untorqued, and the white arrow indicates how the bolted plate swings up to be secured by the left bolt (missing in image).	6
Fig. 5	CAD image showing the region of uniform stress distribution and intended location of failure, as indicated by the double-ended yellow arrow, circumstances under which the test is deemed “valid”.....	7
Fig. 6	Rendered CAD images showing the specimen clamping mechanism of the stationary grip with a) both bolts tightened (yellow arrows), b) left bolt tightened and right left loose, and c) and d) corresponding FEA images showing the stress distribution. Note a stress concentration at the right grip in c), whereas the same grip in d) is stress-free. Inset of (c) shows real-life photo of specimen failure at stress concentrator as indicated by FEA.	7
Fig. 7	Examples of several fractured specimens (with right bolt untorqued at stationary grip). Note these are unpolished specimens used purely for validation of the clamping mechanism.	8
Fig. 8	Finite element images of stress distribution across specimen a) with fillets at the shoulder region, b) without fillets, and c) with groove showing corresponding stress concentration. d) Photo of (unpolished) specimen post-failure along groove.	9
Fig. 9	Toolpath generated in SOLIDWORKS for machining the fatigue specimens. Rolling direction is indicated.	9
Fig. 10	Rendered CAD image showing the mechanism for adjusting the expansion rod.....	11
Fig. 11	High-cycle fatigue data comparing this work with several literature works.....	16

Acknowledgments

The authors thank Dr Rajiv Mishra for providing the original plans for the fatigue tester, and Dr Kaimiao Liu for helpful correspondence during development of the fatigue tester at DEVCOM ARL. Dr Mishra's research group owns several instruments similar to the one reported herein and have successfully used them to generate valuable material data and published works.

The authors would also like to thank the College Qualified Leaders program managed by Army Educational Outreach Program for facilitating the co-op internship opportunity under which this research was carried out. The development of the fatigue tester was carried out over the course of two summer co-ops and one short winter break.

1. Introduction

Mechanical failures exist across several disciplines of engineering and can occur in a variety of components of structures. Failure due to fatigue, in particular, is the most common—responsible for up to 90% of metallic failures in structural materials¹—and can lead to extensive damages. As fatigue of materials is still only partly understood, proper fatigue design could significantly mitigate the impact of these failures. Today, with the continued development of high-strength materials and demand for higher performance, fatigue analysis has assumed an even greater role in material characterization and the engineering pipeline of mechanical components.

Fatigue data provides information on the ability of materials to resist cracking under conditions of repeated strain cycling and can be used as a research and development tool for alloy design. Thus far, the majority of fatigue testing is conducted using conventional, full-scale infrastructure. Here we develop and validate a small-scale fatigue test bed to be used to generate stress amplitude S versus cycles to failure N (S - N) diagrams. While the instrumentation and machinery for full-scale testing is developed, that for small-scale testing is much less ubiquitous, with fewer standardized procedures for use. A small-scale tester, however, is particularly useful for materials subjected to volume constraints and for evaluating novel materials in a first-order manner prior to having to invest in larger-scale material production and costly specimen preparation. For instance, with recent advancements in material discovery driven by the emergence of high-throughput approaches, a small-scale fatigue tester would be particularly useful for supplementing material property evaluations (e.g., for additively manufactured materials).

2. Description of Instrument

2.1 Basic Operation

Fatigue tests were carried out in the spirit of ASTM standards B593 and E739,^{2,3} which establish requirements for the reversed and repeated bending fatigue of flat sheets by fixed cantilever, constant deflection-type testing machines generally limited to a fatigue life range of 10^5 – 10^8 cycles. The specimen is held at one end, acting as a cantilever beam, and deflected by a concentrated load applied at the other end vis-à-vis a regular sinusoidal stress until failure or run-out. The number of cycles to failure is recorded as a measure of fatigue life. All the tests herein were conducted in air at room temperature with a nominal stress ratio of $R = -1$ (mean

displacement equal to 0) although the instrument is capable of achieving stress ratios anywhere between -1 (“fully reversed” condition) and 0 (“pulsating tension” condition) by adjusting one or more components.

The monitoring system used to provide a direct read-out of the number of cycles is controlled by a LabVIEW interface programmed to record the stress waveform, which is calculated from the specimen thickness input by the user prior to the test. The code provides the user with data on the intermediate incremental maximum and minimum stress values of each cycle along with the corresponding number of cycles and timestamp. All data is output into a comma-separated value (CSV) file for further analysis.

Note the present instrument has been adapted from original design plans (documented for aluminum [Al] alloy 7075 in Mishra et al.⁴) received from Dr Rajiv Mishra (University of North Texas). Significant modifications have been made to the physical tester and the LabVIEW software required to operate it to accommodate our needs.

2.2 Mechanical Linkage

Figure 1 displays a rendered image of the instrument with all parts labeled. The tester works on the principle of a treadle linkage, converting rotary motion into oscillatory motion; the mechanical linkage operates similarly with a crank-rocker mechanism. The motor input drives a set of two cams: the outer cam and an inset cam offset from the outer cam. During test setup, shown in Fig. 2, counter rotation of the cams adjusts the radial distance between the link (i.e., ball joint) and the motor axis, which controls the stroke length (i.e., stress amplitude). For instance, the farther the link is away from the motor axis, the longer the stroke length. The cams are adjusted by loosening the set screw of the outer cam and counter-rotating the inset cam.

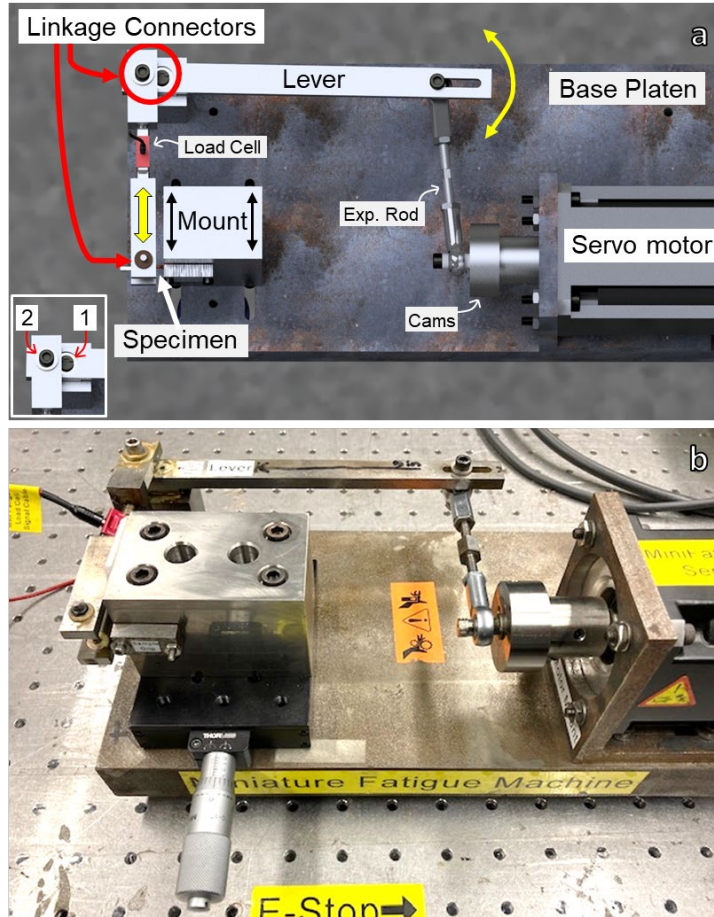


Fig. 1 Overview images of the fatigue tester with key parts labeled in a) rendered form (top-down) and b) a photograph (at an angle)

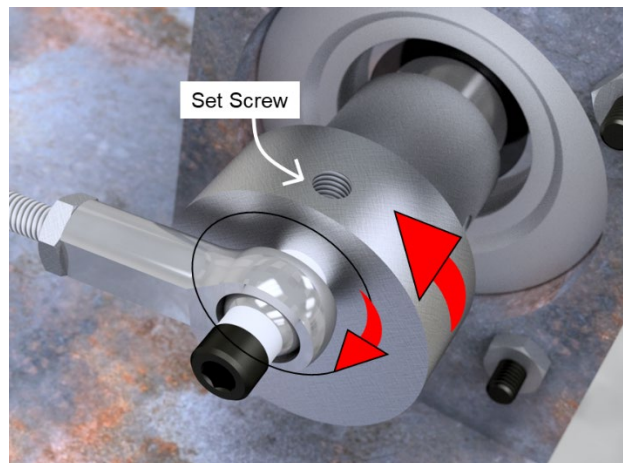


Fig. 2 Rendered CAD image showing counter-rotation adjustment of the cam housing

The motor–cam mechanism can be simplified to a crank link, the length of which is controlled by the cam adjustment. The crank drives an expansion rod of

adjustable length (Fig. 1) with ball joints at both ends. The expansion rod drives the lever arm on one end; on the other end (left side in Fig. 1) the lever arm pivots about Linkage Connector 1 (inset image). Linkage Connector 1 is located considerably closer to the fixed pivot (Linkage Connector 2) than the opposite end of the level arm where the ball joint is located, which reduces the linear displacement by a factor of 16.

The slot on the ball-joint end of the lever arm permits adjustment of the effective length of the lever arm, as the expansion rod can be secured at any position within the slot. This is one way the stress amplitude can be tuned (see Section 2.4.1). The last link contains the load cell, which is attached at one end to the lever arm via Linkage Connector 2 (Fig. 1 inset). The load cell measures the axial load undergone by the link and thus the bending load on the specimen. The other side of the link is attached to the side of the specimen that deflects. In fact, the specimen itself acts as a “link” as it constrains the motion of the load cell link to a single plane (in the direction of the yellow arrow). The length of the specimen is comparable to the distance between Linkage Connectors 1 and 2, which makes the slight (<0.001 inch) out-of-plane displacement useful, as it mirrors the displacement of the link.

Several reasons exist for using a rotary device to drive axial motion. First, sourcing a high-performance servomotor is straight-forward and cost-effective, whereas linear actuators for subscale testing are less common and usually much higher in cost. A piezoelectric-driven linear motor, for instance, also has much more-extensive driver requirements in addition to the aforementioned shortcomings. Most linear actuators are designed for alignment and cannot operate at high speed, whereas servomotors are equipped to offer prolonged precision at high speeds, making them particularly useful for high-cycle fatigue testing. The advantages of using a servomotor are clear for the purposes of this work, although other methods have been explored by other researchers and proven successful (e.g., using a voice coil from a subwoofer as a driver).⁵

To ensure consistent specimen deflection with each cycle during a test, the displacement of the specimen was measured at the mobile grip with a micrometer probe. Across multiple manually driven cycles (rotating the outer cam by hand), the displacement was measured to be the same within the precision of the gauge (the thousandth of an inch). The only source of fluctuating displacement would be the introduction of any mechanical backlash (i.e., bearing/bushing wear, which would most likely be consistent throughout a test).

2.3 Description of Specimen

2.3.1 Design

The specimen is a flat sheet subscale dog-bone of modified Krouse-type geometry.² As shown in Fig. 3, the specimen has an asymmetric gauge section that tapers to form a 20° angle between the two sides and expanded grips at either end, one larger than the other. The larger end (right in Fig. 4a) is situated in the “stationary grip” labeled in Fig. 4a. Here, the specimen remains immobile and is clamped with a bolted plate. The left bolt is tightened with a calibrated torque wrench to 5 inch-lb, and the right bolt is left loose but secured. The smaller end of the grips (left in Fig. 4a) is situated in the “mobile grip”, which undergoes axial motion in and out of the plane of the specimen (in the direction of the double-ended yellow arrow in Fig. 1), therefore subjecting the specimen to plane bending. At this end, the specimen is sandwiched between a small T-shaped plate and rod that is about 2.5 mm in diameter, as shown by the angled view in Fig. 4b, all of which are secured in place with two small bolts tightened alternately to 1.5 inch-lb to ensure consistent gripping between tests. A 1/32-inch pin is inserted between the two bolts through the T-shaped plate, specimen, and rod in that order. The pin functions mainly as an alignment guide and does not bear much load throughout the test. It is left inserted for the duration of the test; in the event that it falls out, it is not re-inserted prior to the test ending. The rod extends vertically through the opening and is held in place by an oil-embedded bushing and O-ring. The O-ring does not bear any load in the test and is only there to hold the rod in place when the sample is removed.

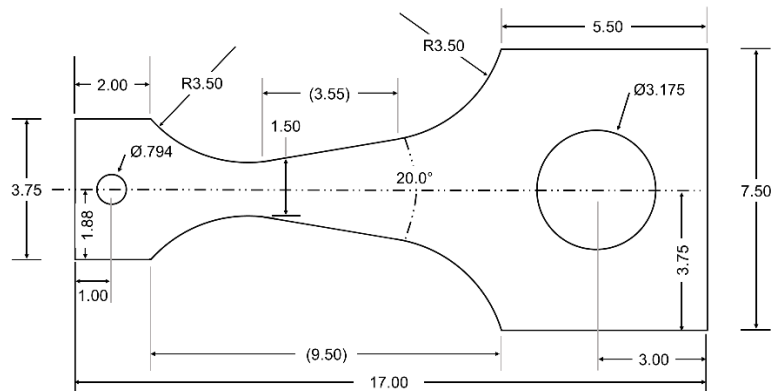


Fig. 3 Schematic showing specimen geometry (millimeters). The two holes are machined with imperial units: 1/32 and 1/8 inch (left to right); equivalent dimensions shown in metric.

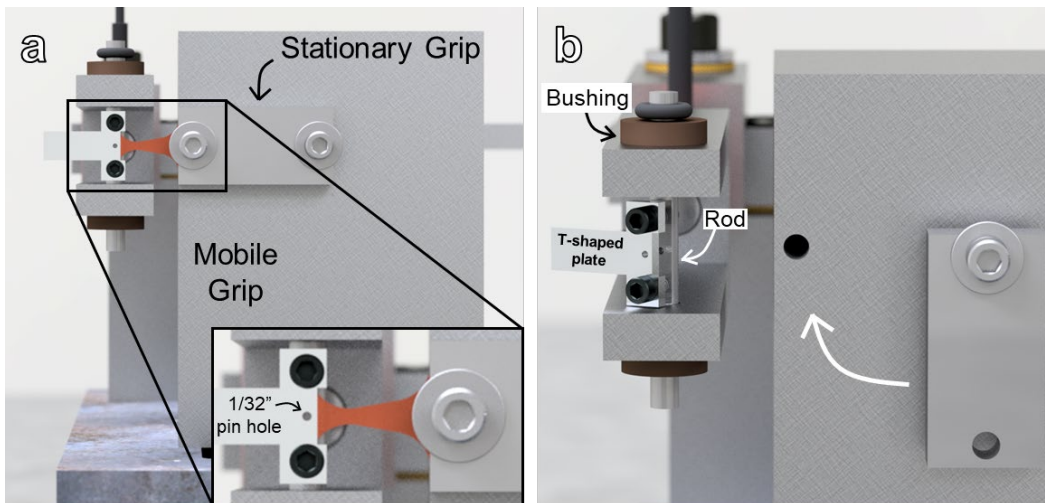


Fig. 4 Rendered CAD images showing the clamping mechanism with a) a specimen present (orange) and b) the specimen missing with an angled view of the mobile grip. The stationary grip is untorqued, and the white arrow indicates how the bolted plate swings up to be secured by the left bolt (missing in image).

Here at the mobile grip, as the load is applied at the point at which the two sides of the gauge section converge, the specimen is in essence a cantilever beam and can be tested in plane bending with a stress ratio up to $R = -1$ (fully reversed loading condition). An added benefit of cantilever bend loading (and subscale specimens) is that it generates less heat due to cyclic loading than axial loading and larger specimens.⁶

2.3.2 Stress Distribution

In cantilever bending mode the tapered geometry concentrates the maximum stress uniformly along the gauge length (yellow double-ended arrow in Fig. 5).⁷ In fact, a benefit of cantilever beam machines is that the uniform stress distribution requires smaller loads than for uniform bending or axial fatigue of the same size sample. The mechanism used to grip the specimen should maintain this stress condition, thus confining failure to this region. If failure occurs elsewhere, the test is deemed invalid because the data is unreliable. When the tester was being developed, failure occurred in the region of the 1/8-inch hole at the stationary grip (inset of Fig. 6c), which motivated further investigation via finite element analysis (FEA) to understand the cause.

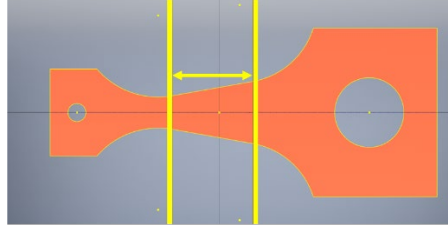


Fig. 5 CAD image showing the region of uniform stress distribution and intended location of failure, as indicated by the double-ended yellow arrow, circumstances under which the test is deemed “valid”

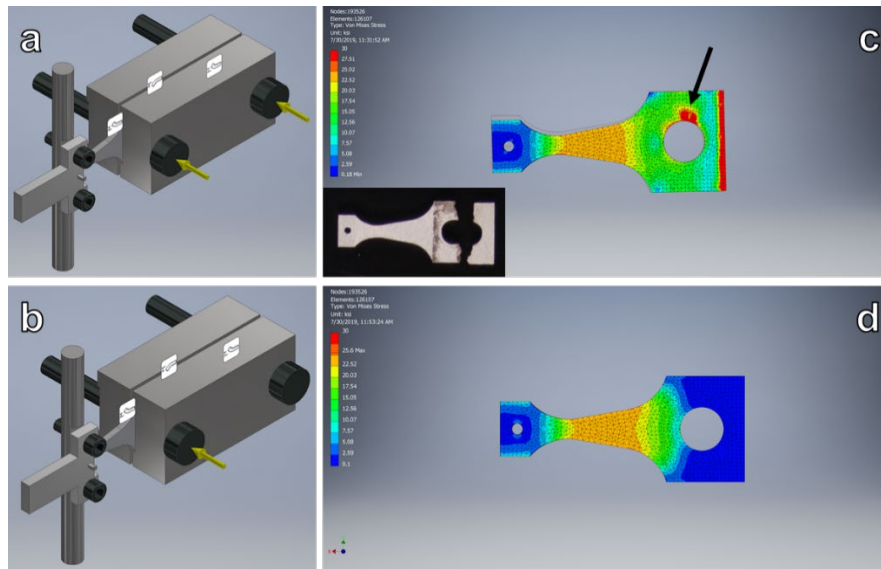


Fig. 6 Rendered CAD images showing the specimen clamping mechanism of the stationary grip with a) both bolts tightened (yellow arrows), b) left bolt tightened and right left loose, and c) and d) corresponding FEA images showing the stress distribution. Note a stress concentration at the right grip in c), whereas the same grip in d) is stress-free. Inset of (c) shows real-life photo of specimen failure at stress concentrator as indicated by FEA.

The specimen grips were generated in the CAD application Autodesk Inventor (Fig. 6a and b). The stationary grip was grounded with the appropriate clamping force based on the specified torque (as mentioned in Section 2.3.1). The mobile grip was clamped with the same considerations, adding the force of gravity. Additionally, the rod the specimen is mounted to has an applied bearing force—the magnitude of which was chosen to achieve the desired displacement in the model—albeit of little importance, as it does not alter how the stress is distributed across the gauge section.

Fig. 6a shows the stationary grip where both bolts are grounded with the same force (yellow arrows), whereas Fig. 6b shows the image where only the left bolt is grounded (single yellow arrow). The corresponding stress distribution is shown in

the FEA images in Fig. 6c and 6d, respectively. At first, both bolts were torqued in practice, as this was believed to most effectively stabilize the grip. However, this mode of clamping introduced a stress concentrator at the 1/8-inch hole, as shown by the black arrow in Fig. 6c, as is common for specimens with geometric irregularities.⁷ Thus, the fatigue strength was reduced significantly, and cracking initiated in this region, leading to the specimen failure shown in the inset of Fig. 6c. In an attempt to restore the uniform stress distribution along the gauge length, the force on the right bolt was removed (Fig. 6b), which consequently eliminated the stress concentrator at the hole (Fig. 6d). Thereafter in practice, the right bolt was left loose prior to testing, which resulted in specimen failure within the gauge section (Fig. 7).

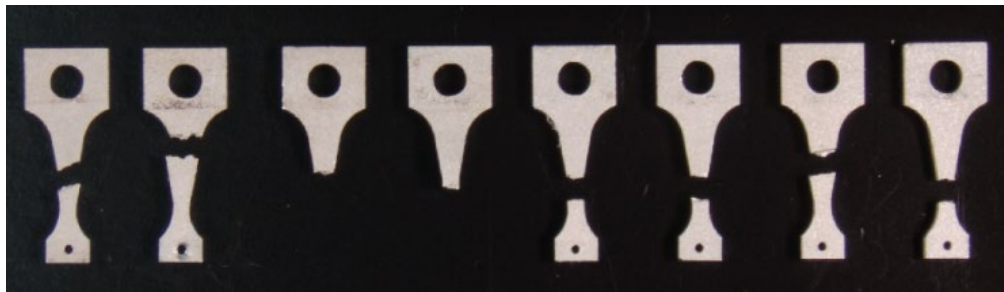


Fig. 7 Examples of several fractured specimens (with right bolt untorqued at stationary grip). Note these are unpolished specimens used purely for validation of the clamping mechanism.

The finite element model was further used to investigate the effect of fillets at the shoulder region in regard to presence of stress concentrators and area coverage of the induced stress. Fig. 8a and 8b show the stress distribution across the specimen with and without fillets (black arrows), respectively. As shown, all stresses are confined within the borders of the grip, and there are no stress concentrators. However, the presence of fillets concentrates the maximum stress more uniformly in the gauge length. The stress distribution is not perfectly uniform in the y-direction (vertical) due to gravity, but these effects are negligible and can be ignored. As a proof of concept, the effect of scratches was examined by notching the gauge section of the dog-bone with a vertical groove, as shown in Fig. 8d. The notch formed a stress concentration (verified with FEA in Fig. 8c), which confined failure to the groove.

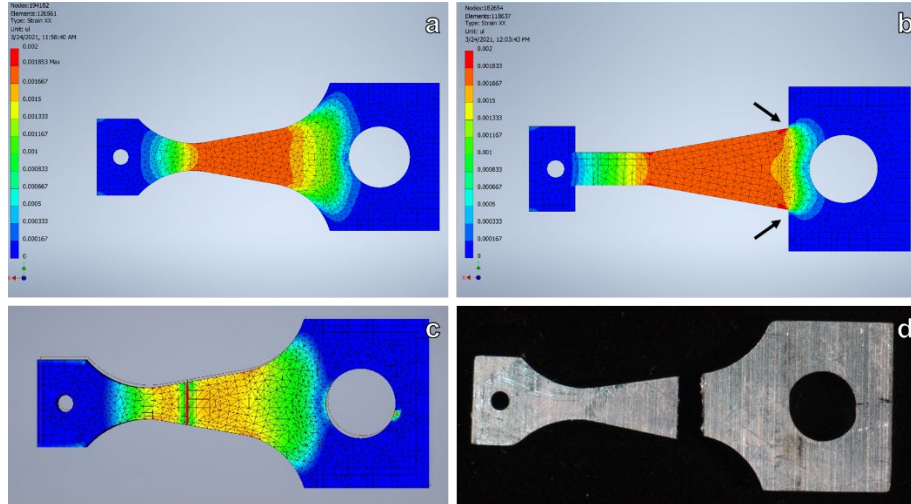


Fig. 8 Finite element images of stress distribution across specimen a) with fillets at the shoulder region, b) without fillets, and c) with groove showing corresponding stress concentration. d) Photo of (unpolished) specimen post-failure along groove.

2.3.3 Specimen Preparation

Subscale fatigue specimens can be prepared from source material of any volume. Here, metal sheets with 1.5 mm thickness were supplied (bulk metal would have to be sectioned into ~1.5 mm sheets). The sheets were superglued to a sacrificial aluminum platen and milled with a Tormach PCNC 1100 CNC machine to the correct geometry using a three-tool operation (via tool changer) with continuous flow of coolant. All dog-bones were machined with the rolling direction in the same longitudinal axis as the gauge length, as indicated by the white double-headed arrow in Fig. 9. As shown in Fig. 9, toolpaths were generated in SOLIDWORKS CAD software with settings (e.g., feed rate and depth of cut) selected with due regard to the material being cut and to yield a high-quality surface finish.

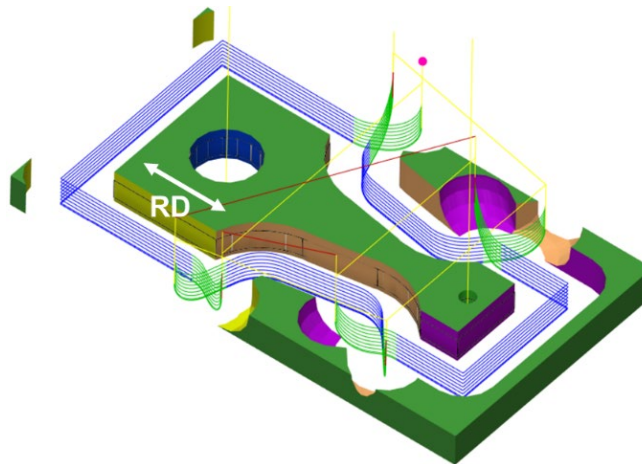


Fig. 9 Toolpath generated in SOLIDWORKS for machining the fatigue specimens. Rolling direction is indicated.

The small and large holes are drilled with 1/32- and 1/8-inch carbide drill bits, respectively, followed by the sides of the gauge section with a 1/8-inch 4-flute titanium-coated carbide end mill. The remainder of the specimen is milled with the same 1/8-inch end mill. While developing the tool path, the 1/8-inch end mill yielded similar surface finish to the 1/32-inch mill while being much more robust (longer tool life). The 4-flute end mills yielded a much smoother surface finish than the 2-flute end mills. Additionally, the high rigidity of the CNC mill greatly improved surface finish.

Both planar surfaces of the specimens were ground and polished using standard metallographic procedures down to 1- μm surface finish and approximately 1.0-mm thickness. It is important that care be exercised, particularly in minimizing effects such as work hardening or induced stress, to prevent alteration of the microstructure.² The sides of the specimen were left as-milled. Care was taken to avoid scratches in the gauge section while handling the specimens.

2.4 Test Setup Procedure

The fatigue tester is adjustable to two main criteria: the loading (or stress) amplitude and the loading center about which the load cycles. Prior to running a test, other than installing the specimen itself, these two criteria need to be set to establish the conditions of the test.

2.4.1 Stress Amplitude Adjustment

The stress amplitude is set by adjusting either the counter-rotation of the cam housing or the effective length of the lever arm. As mentioned, the cam housing is adjusted by rotating the outer cam with respect to the inset cam. The longer the distance between the two cam centers, the higher the effective stress amplitude. The effective length of the lever arm can be adjusted by changing the position at which the ball joint is secured in the slot on the right side of the lever arm pictured in Fig. 1. The longer the effective length of the lever arm, the shorter the distance traveled by the load cell link and thus the less the deflection of the specimen during testing (i.e., lower stress amplitude). The frequency of the load cell can be adjusted between 0.5 and 50 Hz; if the limit is reached, higher stress amplitudes can be achieved simply by reducing the thickness of the specimen.

To generate an S-N curve, total cycles to failure are determined for multiple stress values. The maximum stress value is typically chosen to be up to 90% of the yield strength of the material. Here, the yield strength was determined by preparing separate subscale tension dog-bones for small-scale tension testing, but full-scale tension data could be used as a starting point if known.

2.4.2 Center of Loading Adjustment

The center of loading is set by adjusting the length of the expansion rod and the position of the fixed specimen block. The expansion rod consists of a left-hand thread on one side and a right-hand thread on the other, functioning like a turnbuckle (red arrows in Fig. 10) wherein rotating the rod can adjust its length without disassembly. The length of the rod is locked in place by two jam nuts, as indicated in Fig. 10. The two ends of the rod feature ball joints, which are necessary to accommodate the two planes of motion, although one plane of motion is optimal for design purposes since ball joints are not designed for high cycle use due to excessive wear and accumulation of heat. During the first few rounds of testing, the ball joint wore away the threads on the bolt connected to the motor, effectively decreasing its diameter and encouraging mechanical backlash. The threaded bolt was replaced with a shouldered stainless steel bolt. Future design modifications may include replacing the ball joints altogether with the proper bearings and rotating the motor 90° about its axis relative to the base platen so as to allow the rod to function in a single plane.

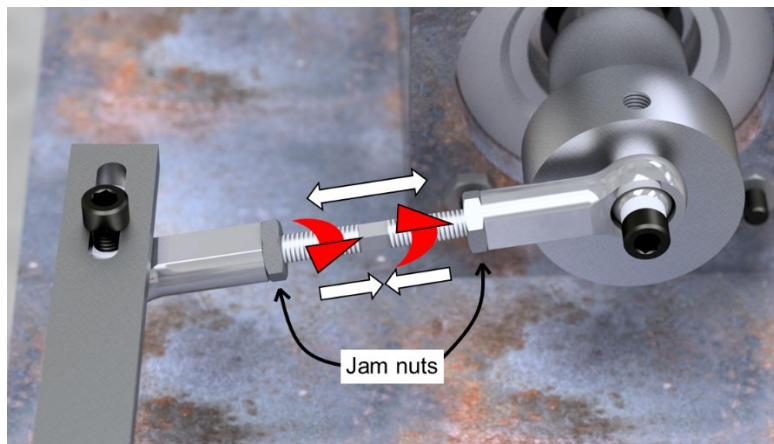


Fig. 10 Rendered CAD image showing the mechanism for adjusting the expansion rod

In addition to the expansion rod, the mounted specimen block can also be used to make adjustments to the center of loading. It can be translated with respect to the base platen in the direction of the black double-ended arrows in Fig. 1, as shown by the slots in the base platen. To move the specimen block more precisely, a Thorlabs translation stage was installed, which makes the adjustment much more convenient and facilitates travel with micrometer accuracy.

2.5 Fracture Mechanics

To correlate the applied load to stress, the maximum bending stress is calculated using the simple beam equation as follows:

$$M = P * L \quad (1)$$

$$I = \frac{1}{12} b * d^3 \quad (2)$$

$$\sigma = \frac{M*x}{I} \quad (3)$$

$$\sigma = \frac{M*x}{I} = \frac{M*\frac{d}{2}}{\frac{1}{12}bd^3} = \frac{6*M}{bd^2} = \frac{6PL}{bd^2} \quad (4)$$

$$\sigma = \frac{6PL}{bd^2} \quad (5)$$

where σ is the bending stress (N/m²), P is the force (N), L is the distance between axis of point of load application and point of stress calculation (m), b is the width of the specimen at distance L from point of load application (m), d is the specimen thickness (m), M is the bending moment, I is the moment of inertia, and x is the distance from the beam neutral axis to the point of interest perpendicular to the neutral axis. Due to the tapered geometry (20° convergence angle, as shown in Fig. 3), the ratio $\frac{L}{b}$ is known, thus the equation simplifies as follows:

$$\frac{L}{b} = \frac{1}{2} * \frac{1}{\tan\left(\frac{1}{2} * 20^\circ\right)} = 2.8356 \quad (6)$$

$$\sigma = 2.8356 * \frac{6P}{d^2}$$

Equation 6 can be used to calculate the maximum stress at the surface of the specimen at any point in the gauge section with knowledge of only the applied load P and specimen thickness d . Prior to testing, the specimen thickness is entered into the LabVIEW user interface. The program then reads the thickness and calculates the stress throughout the test using the measured load (see Section 2.7.2.1 on how the load is collected and processed).

2.6 Maintenance/Wear

After prolonged testing, the mechanical linkage undergoes wear in a few areas, and given the high-frequency nature of the system, the wear can be significant. The oil-embedded bronze bushings that hold the rod in place will deteriorate due to friction over time. The thrust ball bearings (four total) connecting the lever arm and load cell links will fail over the span of multiple tests by fracturing and splitting, as bearings are not designed for partial rotation on the order of sub-10°. Thus, frequent application of grease (even during a test) and taking the bearings through several full rotations between tests will extend their life.

2.7 Electronics

2.7.1 Overview

The electronics for the fatigue tester include the following:

- Kaman Automation S200 Servo driver
- Kollmorgen AKM series brushless servo motor
- Futek 25-lb load cell
- Load cell power supply
- Strain gauge analog amplifier with voltage output (load cell amplifier)
- National Instruments data acquisition (DAQ) card
- NPN transistor, few other resistors
- Emergency stop switch

The servo driver supplies variable frequency three-phase power to the motor (and corrects the speed based on the included feedback sensors). The servo driver interfaces to a computer via serial connection for test setup and velocity adjustments. The driver can be controlled through analog/digital ports to circumvent the computer, which is how the DAQ turns the motor on and off through the LabVIEW interface. To prevent the motor from starting if the DAQ's USB connection is interrupted or a fault occurs, a transistor is integrated to invert the signal—using the DAQ's 15-VDC power supply—and the digital output of the DAQ to create the appropriate digital signal.

The resistors are used to run the transistor circuit. The load cell is connected to the load cell amplifier to excite the Wheatstone bridge and make the force measurable by an analog channel. The load cell amplifier receives external DC power from a power supply. The analog out of the amplifier is connected to a channel on the DAQ. Last, the emergency stop switch is placed to cut AC power to the servo driver and load cell amplifier for safety reasons.

2.7.2 LabVIEW Code

2.7.2.1 Data Collection

The primary function of the LabVIEW code is to record the waveform output by the load cell and process the associated data. For the tests herein, the motor speed was set to 1500 rpm (25-Hz flexing frequency), and the force was sampled 20 times

each cycle to adequately capture the maximum and minimum values in the loading cycle. The sampling rate of 20/cycle is sufficient to prevent aliasing. Sampling and saving at a higher rate is unnecessary and may lead issues with buffering. The data is averaged across a user-specified number of cycles, usually 100, and saved at that interval. The code is programmed to save the averaged maximum, minimum, corresponding number of cycles (as determined by the last cycle of each 20-cycle increment), and timestamp into a CSV file.

The averaged minimum and maximum are imported into Microsoft Excel to calculate the load/stress amplitude, taken as half of the peak-to-peak value. To measure the amplitude, half of the average of all of the peak-to-peak values is taken. The R-value is calculated by dividing the averaged maximums by their corresponding minimums and taking the average of the quotients. Note that since the instrument operates under conditions of constant displacement, the measured load decreases slightly over time as cracks nucleate and grow.⁵ Overall, this saved data allows the user to make correlations between any physical phenomena (e.g., cracking) and, more importantly, ensures that the end of the test is accurately captured. The load read from the load cell is assumed to be the force applied on the specimen. Inertial effects of accelerating the grip are not considered.

2.7.2.2 Automatic Stopping

Automatic stopping was integrated as a design modification for the fatigue tester so as to not require the user to be present at the moment the specimen fails. When the “Break Detect” button is activated in the LabVIEW interface, the motor is signaled to stop when the loading amplitude drops below a user-specified threshold. That threshold should be set at a level above the baseline noise of the machine but below that at which the sample is expected to fail so as to not cause the motor to stop prematurely. This promotes more autonomous operation of the tester and reduces post-rupture damage to the specimen if fractographic examination is of interest. For instance, without automatic stopping, the motor would continue to spin and the load cell link would continue to travel back and forth (and swing outward as it is no longer constrained by an intact specimen). This could put both halves of the specimen in contact with one another. Note the Break Detect function may prematurely end the test at times, but the program can be restarted and the number of cycles from the two tests summed. Usually, premature failure occurs with only a few cycles left in the lifetime of the specimen. It would be rare for the Break Detect function to miss sample failure; however, if this occurs, the saved waveform can be analyzed to find the point of fracture.

2.7.2.3 Modifications

The LabVIEW interface was reprogrammed in its entirety to improve system operation and user friendliness. A streamlined series of modes was established in the following order: setup mode, calibration mode, running mode, and paused mode. The setup mode is active before the code is run and gives the user the opportunity to adjust the channel ports. Upon running the test, the user is prompted for a file name and location, and the system enters the calibration mode thereafter. Here the user inputs the specimen thickness and motor speed and can view a live read-out of the load cell while making adjustments to the cams, expansion rod, and/or specimen block to reach the desired stress waveform criteria.

After the user is satisfied with the adjustments, the start button is pressed and the test begins. Data is saved at the calculated rate based on the input motor speed, and the motor is automatically started. The test can be paused and resumed at any time, which would stop and restart the motor, respectively, and suspend and resume data collection, respectively. Due to the automatic stopping function, the test will automatically stop when the amplitude drops below the user-specified threshold, or in the case of fatigue run-out, the test can be manually stopped via the user interface.

2.8 Instrument Validation

The specimen and instrument design was validated for Al alloy 6061 (T6 temper). Results from this work were compared with those of others tested at full scale under similar conditions. Although it is generally accepted that there is no fatigue limit in Al alloys, based on Suresh,⁸ the fatigue limit has been defined as the stress amplitude the specimen can withstand without failing for at least 10^7 cycles. That of 6061 is quoted as 95 MPa, and yield strength is given as 275 MPa.^{9,10} Although the yield strength measured in this work for 6061 was considerably higher at 309 MPa, as shown in Fig. 11, the fatigue data falls within the range of that in literature works, particularly Takahashi et al.¹¹ and Chanyathunyaraj et al.¹² In Takahashi et al.,¹¹ Chanyathunyaraj et al.,¹² and Almaraz et al.,¹³ testing used rotating bending machines, and in Mutombo and Du Toit,¹⁴ testing was carried out under axial fatigue with the T651 temper instead of T6 (Takahashi et al.,¹¹ Chanyathunyaraj et al.,¹² and Almaraz et al.¹³ were all T6). Mutombo and Du Toit's data differs presumably due to the different mode of testing and temper, but Almaraz et al.¹³ yielded lower fatigue strength despite using similar testing conditions as Takahashi et al.¹¹ and Chanyathunyaraj et al.¹²

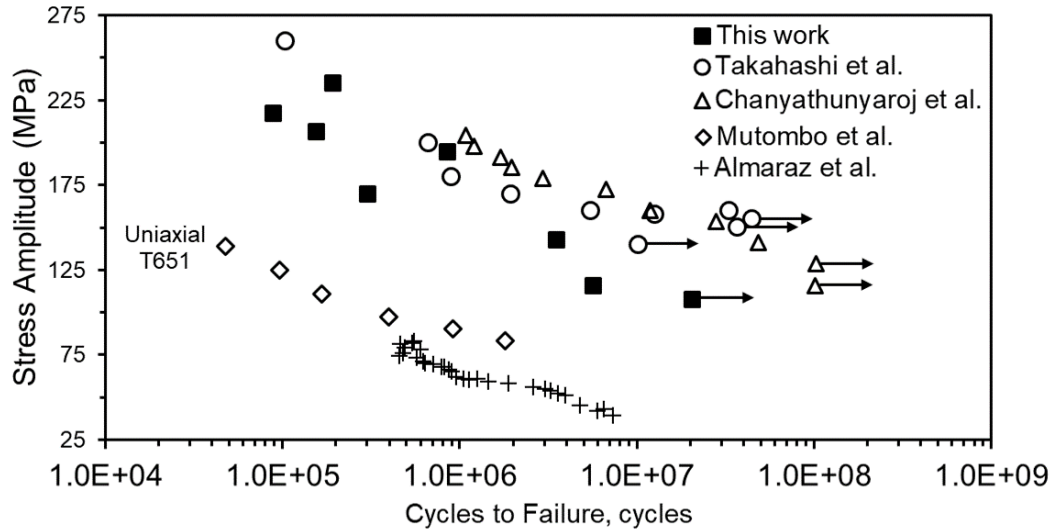


Fig. 11 High-cycle fatigue data comparing this work with several literature works

Fatigue life is highly dependent on material microstructure and testing environment, and when these factors are not controlled, significant scatter and discrepancies can exist in the data. For instance, metallurgical discontinuities or manufacturing imperfections (e.g., pores) in commercial alloys wrought by the forming processes used in their production promote cracking and lead to failure at lower stress levels, as these defects act as stress concentrators.⁹ While they may meet minimum alloy specifications, alloys may also have different material properties (e.g., $\Sigma_V = 358$ MPa in Takahashi et al.¹¹ vs. 270 MPa in Chanyathunyaraj et al.¹²) depending on the manufacturer and location in the bulk material from which samples are taken. Regarding testing environment, as most high-cycle fatigue testing is carried out in uncontrolled ambient-air settings, even atmospheric moisture is recognized to have a corrosive effect on fatigue performance.⁹ Thus, several reasons contribute to scatter when comparing results of different investigations. In this work, although the temperature and humidity level were recorded at the beginning of each test, tests lasted several days or more, and these conditions were not controlled over the course of the test. Future improvements may include placing the tester in a climate-controlled enclosure to minimize fluctuations and thus scatter in the data. Despite these shortcomings, the similarity between the data produced herein and those in the literature is deemed acceptable and thus warrants effective implementation of the test bed in fatigue evaluations of at least Al alloys, but should still be compared with full-scale test literature data if available. At the very least, these subsize specimens can be a useful tool for comparative investigations of fatigue life. In the original version of this tester, Mishra et al. carried out tests on Al alloy 7075 and reported similar results between subsize and standard specimens.⁴

3. Size Effect

As with any evaluation on the subscale, size effects are of concern. Generally, it is well known that the measured strength of a material increases with specimen miniaturization because smaller samples statistically contain fewer defects (inclusions, hard surface particles, etc.), thus lowering the probability of crack initiation. For instance, Tomaszewski et al.¹⁵ demonstrated increased fatigue strength of miniature 6064 Al alloy specimens versus the standard size by almost an order of magnitude in cycles to failure. Despite this prevailing trend, size effects for Al alloy 6061 are not observed in the current study, although this may not apply for a different class of materials. To conduct a full system validation, the instrument should be tested for a variety of materials. Testing of A36 steel is currently ongoing.

4. Conclusion

In this work, a small-scale fatigue tester capable of quantifying high-cycle fatigue via constant amplitude (deflection) loading of metal alloys was developed and validated. The instrument works on the principle of a treadle linkage, converting rotary into oscillatory motion and is designed to conduct fully reversed bending by fixed cantilever limited to a fatigue life range of 10^5 – 10^8 cycles of modified Krouse-type planar specimens. The LabVIEW program written to run the testing has been optimized for user friendliness with features like automatic stopping once the loading amplitude drops below a certain threshold (i.e., a break is detected in the specimen). The instrument has been validated for Al alloy 6061 and demonstrates comparably to literature works using full-scale testing methods. Size effects were not detected for alloy 6061 but, in general, fatigue data can be influenced by a variety of test conditions, so small-scale data should be compared with literature values for verification when possible.

5. References

1. Campbell FC, editor. Elements of metallurgy and engineering alloys. ASM International; 2008.
2. ASTM B593. Standard test method for bending fatigue testing for copper-alloy spring materials. ASTM International; 2021.
3. ASTM E739. Standard practice for statistical analysis of linear or linearized stress-life (S-N) and strain-life (ϵ -N) fatigue data. ASTM International; 2017.
4. Mishra RS, De PS, Obermark CM. Development of a reversible bending fatigue test bed to evaluate bulk properties using sub-size specimens. *J Test Eval*. 2008;36(4):402–405.
5. Parvez, MM, Chen Y, Karnati S, Coward C, Newkirk JW, Liou F. A displacement controlled fatigue test method for additively manufactured materials. *Appl Sci*. 2019;9(16):3226.
6. Stephens RI, Fatemi A, Stephens RR, Fuchs HO. Metal fatigue in engineering. 2nd ed. John Wiley & Sons; 2000. p. 62.
7. Boyer HE, editor. Atlas of fatigue curves. ASM International; 1985.
8. Suresh, S. Fatigue of materials. Cambridge University Press; 1998.
9. Dragolich KS, DiMatteo ND. Fatigue data book: light structural alloys. ASM International; 1994.
10. ASM International Handbook Committee. ASM handbook. Fatigue and fracture; vol. 19. ASM International; 1996.
11. Takahashi, Y, Shikama T, Yoshihara S, Aiupa T, Noguchi H. Study on dominant mechanism of high-cycle fatigue life in 6061-T6 aluminum alloy through microanalyses of microstructurally small cracks. *Acta Materialia*. 2012;60(6–7):2554–2567.
12. Chanyathunyaraj, K, Phetchcrai S, Laungsopapun G, Rengsomboon A. Fatigue characteristics of 6061 aluminum alloy subject to 3.5% NaCl environment. *Int J Fatigue*. 2020;133:105420.
13. Almaraz GM, Dominguez VH, Lemus M, Villalon Lopez JJ. Effect of proximity and dimension of two artificial pitting holes on the fatigue endurance of aluminum alloy AISI 6061-T6 under rotating bending fatigue tests. *Metallurg Mater Trans A*. 2012;43(8):2771–2776.

14. Mutombo K, Du Toit M. Corrosion fatigue behavior of aluminum alloy 6061-T651 welded using fully automatic gas metal arc welding and ER5183 filler alloy. *Int J Fatigue*. 2011; 33(12):1539–1547.
15. Tomaszewski T, Sempruch J, Piątkowski T. Verification of selected models of the size effect based on high-cycle fatigue testing on mini specimens made of EN AW-6063 aluminum alloy. *J Theor Appl Mech*. 2014;52.

List of Symbols, Abbreviations, and Acronyms

AC	alternating current
Al	aluminum
ARL	Army Research Laboratory
CAD	computer-aided design
CNC	computer numerical control
CSV	comma-separated value
DAQ	data acquisition
DC	direct current
DEVCOM	US Army Combat Capabilities Development Command
FEA	finite element analysis
NPN	negative-positive-negative
S-N	stress amplitude S versus cycles to failure N
USB	Universal Serial Bus
VDC	volts direct current

1 DEFENSE TECHNICAL
(PDF) INFORMATION CTR
DTIC OCA

1 DEVCOM ARL
(PDF) FCDD RLD DCI
TECH LIB

1 DEVCOM ARL
(PDF) FCDD RLW MF
D YIN